

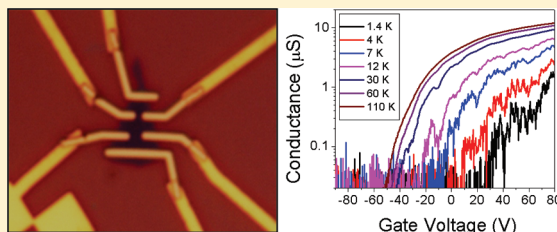
Insulating Behavior in Ultrathin Bismuth Selenide Field Effect Transistors

Sungjae Cho, Nicholas P. Butch, Johnpierre Paglione, and Michael S. Fuhrer*

Center for Nanophysics and Advanced Materials, University of Maryland, College Park, Maryland 20742-4111, United States

ABSTRACT: Ultrathin (approximately three quintuple layer) field-effect transistors (FETs) of topological insulator Bi_2Se_3 are prepared by mechanical exfoliation on 300 nm SiO_2/Si substrates. Temperature- and gate-voltage-dependent conductance measurements show that ultrathin Bi_2Se_3 FETs are n-type and have a clear OFF state at negative gate voltage, with activated temperature-dependent conductance and energy barriers up to 250 meV.

KEYWORDS: topological insulator, bismuth selenide, surface state, field-effect transistor



Topological insulators are a new class of materials that have a bulk band gap and gapless Dirac surface states which are topologically protected from back scattering or localization by time-reversal symmetry. The existence of surface states in Bi_2Se_3 was observed recently by angle-resolved photoemission spectroscopy (ARPES)^{1–3} and scanning tunneling spectroscopy (STS).^{4–6} ARPES measurements indicate Bi_2Se_3 has 0.3 eV bulk band gap and a single Dirac cone surface state in the gap; however, electronic transport experiments which are dominated by surface state transport remain elusive,^{7–10} due to bulk conduction in Bi_2Se_3 .

One strategy to reduce the contribution of bulk conduction is to fabricate very thin Bi_2Se_3 layers, and some electronic transport experiments on thin Bi_2Se_3 films^{11,12} and crystals^{13,14} have been reported. An interesting question is: How thin can Bi_2Se_3 be while retaining its three-dimensional topological insulator character? The thinnest layer that maintains a 2:3 Bi:Se stoichiometry is the quintuple layer (QL) of five alternating Se and Bi planes, while the thinnest slab which retains the symmetry of bulk Bi_2Se_3 is one unit cell, or three QL units, thick. Theoretical work^{15–17} as well as ARPES experiments¹⁸ indicate that in few-QL Bi_2Se_3 the surface states may hybridize and open a bulk energy gap, resulting in either a two-dimensional insulator or a quantum spin Hall system with insulating bulk and conducting chiral one-dimensional edge modes^{19–21}. Here, we report electrical measurements on ultrathin (~ 1 unit cell, or ~ 3 QLs) Bi_2Se_3 crystals as a function of gate voltage and temperature. We observe clear insulating behavior beyond a threshold gate voltage, with activated energy gaps up to 250 meV. The results indicate that ~ 3 QL Bi_2Se_3 crystals are conventional insulators with energy gaps exceeding 250 meV.

Bi_2Se_3 crystals were prepared as described in ref 7. Bulk carrier concentrations (n-type) were in the range of $(2–4) \times 10^{18} \text{ cm}^{-3}$. Bi_2Se_3 was mechanically exfoliated on substrate of 300 nm SiO_2 over a conducting Si back gate using a “Scotch tape” method similar to that used for graphene.²² Figure 1a shows an optical micrograph of a typical mechanically exfoliated Bi_2Se_3 crystal on SiO_2/Si . Crystals of thickness 3.5–30 nm were found

and could be differentiated by color contrast similar to few-layer graphene.²³ The thickness of the samples was measured by atomic force microscopy (AFM), which may overestimate the true thickness of the crystal as is observed for graphene on SiO_2 .²³ The thinnest samples (thickness $t = 3.5$ nm, corresponding to approximately three QLs) were chosen for this study. Electron beam lithography was used to define Pd electrodes; Figure 1b shows the completed device. No adhesion layer was used; we found that using Cr or Ti as an adhesion layer makes contact resistance increase rapidly with time, which might be related to oxidation of the adhesion layer.

Figure 2 shows the gate voltage (V_g) dependent transport properties of four Bi_2Se_3 transistors of various thicknesses. For thicker samples (sample 1, $t = 14$ nm; sample 2, $t = 6.5$ nm), the sheet conductivity measured in a four-probe configuration is shown. For the thinnest samples (samples 3 and 4, $t = 3.5$ nm) the two-probe conductance is shown as a function of V_g . Because of the high sample resistance at low temperatures and negative V_g , we were unable to perform four-probe measurements on the thinnest samples. We always observe n-type doping in exfoliated Bi_2Se_3 , and for samples 1 and 2 the carrier density n determined by the Hall effect at $V_g = 0$, $n = 1.5 \times 10^{13} \text{ cm}^{-2}$ for sample 1 and $n = 2.5 \times 10^{13} \text{ cm}^{-2}$ for sample 2, exceeds the density of the surface state at the conduction band edge ($\sim 5 \times 10^{12} \text{ cm}^{-2}$ for one surface or $1 \times 10^{13} \text{ cm}^{-2}$ for top and bottom surfaces^{1,3}) indicating that the bulk conduction band must also be populated. The Hall mobility is 1200 and 300 $\text{cm}^2/(\text{V s})$ for samples 1 and 2, respectively, at $V_g = 0$. The gate-voltage-dependent transport in samples 1 and 2 is qualitatively similar to that observed by other groups for thicker exfoliated crystals^{13,14} and films.¹² While weakly (logarithmically) insulating behavior has been observed in thin Bi_2Se_3 films,^{12,24} the observation here of transistor-like behavior and a strong (exponentially) insulating state in the thinnest samples is novel, and below we will focus on this behavior in more detail.

Received: January 3, 2011

Revised: April 7, 2011

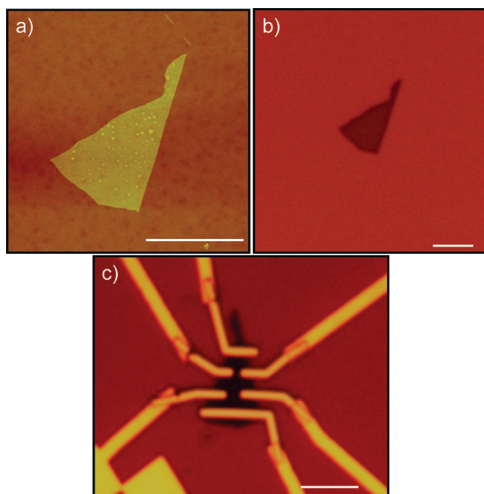


Figure 1. Atomic force micrograph (a) and optical micrographs (b, c) of a 3.5 nm thick exfoliated Bi_2Se_3 sample on SiO_2/Si substrate. Panel c shows the completed device with Pd electrodes contacting the device and larger Cr/Au electrodes leading to bonding pads. Scale bars in (a–c) represent $4\ \mu\text{m}$.

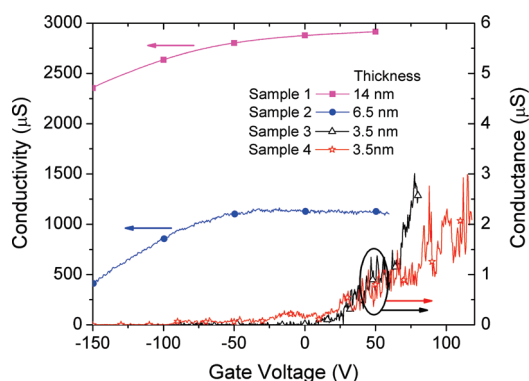


Figure 2. Gate-voltage-dependent transport in four exfoliated Bi_2Se_3 samples. For thicker samples 1 and 2, the four-probe conductivity (left axis) as a function of gate voltage is shown. For thinner samples 3 and 4, the two-probe conductance (right axis) as a function of gate voltage is shown.

Panels a and b of Figure 3 show the two-probe conductance of sample 3 as a function of gate voltage $G(V_g)$ at various temperatures, T showing n-type field effect behavior. (Similar results were obtained for sample 4.) At high T (245–320 K, Figure 3a) we observe that for positive (negative) V_g , the conductance increases (decreases) with decreasing temperature, indicating metallic (insulating) behavior. At lower temperatures (Figure 3b) the conductance decreases with decreasing temperature at all gate voltages. The maximum field effect mobility is $\sim 10\ \text{cm}^2/(\text{V s})$ at $T = 245\ \text{K}$.

Panels c and d of Figure 3 show the conductance data from panels a and b of Figure 2 on an Arrhenius plot. At negative gate voltage (Figure 2c), strongly activated temperature-dependent conductance is observed; straight lines are fits to $G(V_g) = G_0 e^{-E_a/kT}$ where E_a is the activation energy, k is Boltzmann's constant, and G_0 a constant prefactor. At positive V_g and lower temperatures (Figure 2d), activated behavior is also seen with much smaller activation energies.

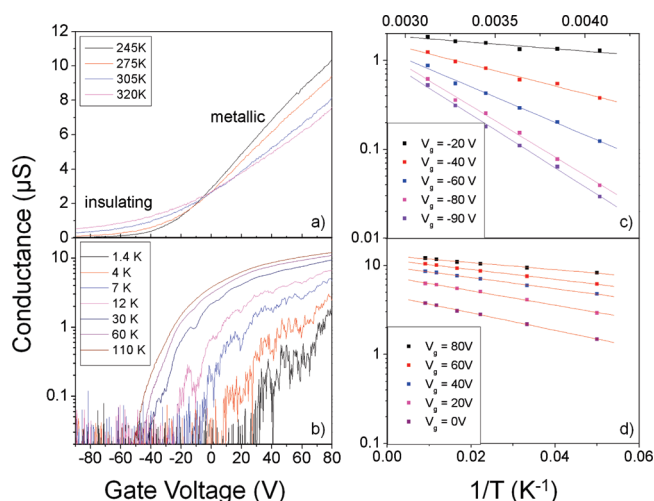


Figure 3. Temperature-dependent conductance of 3.5 nm thick exfoliated Bi_2Se_3 on SiO_2/Si . (a, b) Conductance of sample 3 vs gate voltage at various temperatures. (c, d) Conductance of sample 3 vs inverse temperature on a semilog scale (Arrhenius plot) showing activated behavior. Lines are linear fits to the data.

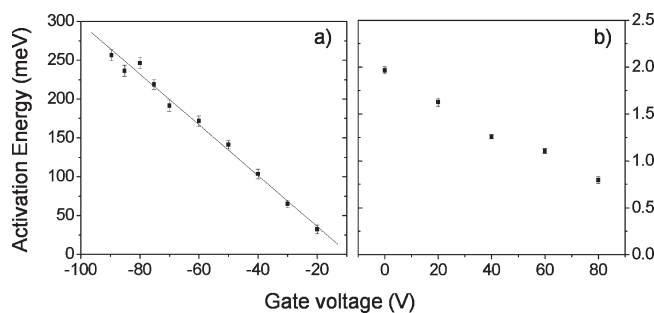


Figure 4. Activation energy as a function of gate voltage determined from fits in panels c and d of Figure 3.

Panels a and b of Figure 4 show the gate-voltage dependence of the activation energies extracted from panels c and d of Figure 3. For negative gate voltages, the activation energy rises roughly linearly with gate voltage, extrapolating to zero at a threshold $V_g = -10\ \text{V}$, and rising to 250 meV at $V_g = -90\ \text{V}$. We interpret the activation energy in this regime as arising due to a barrier to conduction in the bulk, i.e., bulk insulating behavior. (We find the possibility of the activation barrier arising from an insulating contact to a metallic surface state extremely unlikely; first, we observe Ohmic contacts similarly fabricated on slightly thicker Bi_2Se_3 , and second, we cannot imagine a scenario in which the contact, which lies on top of the sample, could show activation behavior continuously tuned by gate voltage from metallic to insulating.) We assume the activated behavior arises from activation of electrons from the Fermi energy, E_F to conduction band edge, E_C ; that is $E_a = E_C - E_F$. Then the variation of E_a with V_g reflects the variation of E_F : $dE_F/d(eV_g) = -dE_a/d(eV_g)$. The fact that the slope $dE_F/d(eV_g) \ll 1$ indicates movement of Fermi level with back gate through localized impurity states in the band gap. A change in the electrochemical potential of the gate $e\Delta V_g$ is the sum of the electrostatic potential change $e\Delta\phi$ and the Fermi energy change ΔE_F : $e\Delta V_g = e\Delta\phi + \Delta E_F = e^2\Delta n/C_g + e^2\Delta n/C_t$ where Δn is the change in charge number density, $C_g = 1.15 \times 10^{-8}\ \text{F}/\text{cm}^2$ is the oxide capacitance

per unit area, and $C_t = e^2 D(E)$ is the quantum capacitance associated with a density of localized states $D(E)$. Then the slope $dE_F/d(eV_g) = C_g/(C_g + C_t)$. From the slope $dE_F/d(eV_g) = 3.3 \times 10^{-3}$, we can estimate $D(E) = 2.1 \times 10^{13} \text{ eV}^{-1} \text{ cm}^{-2}$, and the total charge depleted at $V_g = -90 \text{ V}$ is estimated as $5 \times 10^{12} \text{ cm}^{-2}$ from the bandwidth 250 meV. It is notable that similar behavior was observed in another exfoliated transition-metal chalcogenide, conventional semiconductor MoS_2 FETs on SiO_2 ,²⁵ where field-effect mobilities of $10\text{--}50 \text{ cm}^2/(\text{V s})$ and a localized state density of $7 \times 10^{12} \text{ eV}^{-1} \text{ cm}^{-2}$ were measured. Below $T = 110 \text{ K}$, activated conduction behavior is seen even at positive gate voltage (Figure 3b) and the activation energy is plotted in Figure 4b. We attribute the very small activation energies in Figure 3b to a small Schottky barrier between the Pd contacts and the insulating ultrathin Bi_2Se_3 .

The energy barrier in our ultrathin Bi_2Se_3 FETs is surprisingly large, approaching the bulk energy gap of $\sim 300 \text{ meV}$. We interpret the activation energy as arising from an insulating state in the Bi_2Se_3 , due to coupling of the top and bottom surface states. The magnitude of the energy gap is somewhat larger than the gap of $5\text{--}50 \text{ meV}$ theoretically predicted for 3 QL Bi_2Se_3 ^{15–17} and the gap of 130 meV observed for 3 QL Bi_2Se_3 by ARPES experiments,¹⁸ though it is comparable to the measured gap for 2 QL Bi_2Se_3 .¹⁸ This suggests that the significant density of localized states $D(E) = 2.1 \times 10^{13} \text{ eV}^{-1} \text{ cm}^{-2}$ observed in our experiment may reflect localization of the surface-state-derived bands (which are no longer topologically protected from localization) and conduction may occur in the bulk quantum-well states which should be separated by a gap significantly larger than the bulk gap of 300 meV.

The absence of any p-type conduction channel observed up to $V_g = -90 \text{ V}$ indicates that the actual transport gap may be even larger than 250 meV; in principle one would expect that the high-workfunction Pd contacts would show a smaller barrier for p-type injection. The observation of conductance $G < 10 \text{ nS}$ corresponds to a mean free path for any one-dimensional edge modes $< 1 \text{ nm}$; we therefore conclude that it is unlikely that the ultrathin Bi_2Se_3 is in the quantum spin Hall state.

In conclusion, we have fabricated field-effect transistors from ultrathin Bi_2Se_3 crystals obtained by mechanical exfoliation. The Bi_2Se_3 FETs show n-type behavior, with a clear insulating OFF state and energy barriers up to 250 meV. The small subthreshold swing indicates a large density of trap states $D(E) = 2.1 \times 10^{13} \text{ eV}^{-1} \text{ cm}^{-2}$. The observation of a true insulating state in topological insulator Bi_2Se_3 is presumed to be due to coupling of the top and bottom surface states, resulting in a conventional two-dimensional insulator.

AUTHOR INFORMATION

Corresponding Author

*E-mail: mfuhrer@umd.edu.

ACKNOWLEDGMENT

We acknowledge support from the UMD-NSF-MRSEC Grant DMR-05-20471. N.P.B. acknowledges support from CNAM.

REFERENCES

(1) Hsieh, D.; Xia, Y.; Qian, D.; Wray, L.; Dil, J. H.; Meier, F.; Osterwalder, J.; Patthey, L.; Checkelsky, J. G.; Ong, N. P.; Fedorov,

A. V.; Lin, H.; Bansil, A.; Grauer, D.; Hor, Y. S.; Cava, R. J.; Hasan, M. *Nature* **2009**, *460* (7259), 1101–1105.

(2) Chen, Y. L.; Analytis, J. G.; Chu, J. H.; Liu, Z. K.; Mo, S. K.; Qi, X. L.; Zhang, H. J.; Lu, D. H.; Dai, X.; Fang, Z.; Zhang, S. C.; Fisher, I. R.; Hussain, Z.; Shen, Z. X. *Science* **2009**, *325* (5937), 178–181.

(3) Xia, Y.; Qian, D.; Hsieh, D.; Wray, L.; Pal, A.; Lin, H.; Bansil, A.; Grauer, D.; Hor, Y. S.; Cava, R. J.; Hasan, M. Z. *Nat. Phys.* **2009**, *5* (6), 398–402.

(4) Hanaguri, T.; Igarashi, K.; Kawamura, M.; Takagi, H.; Sasagawa, T. *Phys. Rev. B* **2010**, *82*, 081305.

(5) Roushan, P.; Seo, J.; Parker, C. V.; Hor, Y. S.; Hsieh, D.; Qian, D.; Richardella, A.; Hasan, M. Z.; Cava, R. J.; Yazdani, A. *Nature* **2009**, *460* (7259), 1106–1109.

(6) Zhang, T.; Cheng, P.; Chen, X.; Jia, J.; Wang, L.; Zhang, H.; Dai, X.; Fang, Z.; Xie, X.; Xue, Q. *Phys. Rev. Lett.* **2009**, *103*, 266803.

(7) Butch, N. P.; Kirshenbaum, K.; Syers, P.; Sushkov, A. B.; Jenkins, G. S.; Drew, H. D.; Paglione, J. *Phys. Rev. B* **2010**, *81*, 241301.

(8) Qu, D.-X.; Hor, Y. S.; Xiong, J.; Cava, R. J.; Ong, N. P. *Science* **2010**, *329* (5993), 821–824.

(9) Jenkins, G. S.; Sushkov, A. B.; Schmadel, D. C.; Butch, N. P.; Syers, P.; Paglione, J.; Drew, H. D. *Phys. Rev. B* **2010**, *82*, 125120.

(10) Sushkov, A. B.; Jenkins, G. S.; Schmadel, D. C.; Butch, N. P.; Paglione, J.; Drew, H. D. *Phys. Rev. B* **2010**, *82*, 125110.

(11) Qu, D.-X.; Hor, Y. S.; Li, J.; Ubaldini, A.; Couto, N. J. G.; Giannini, E.; Morpurgo, A. F. *Arxiv:1101.2352*, 2011.

(12) Liu, M.; Chang, C.; Zhang, Z.; Zhang, Y.; Ruan, W.; He, K.; Wang, L.; Chen, X.; Jia, J.; Zhang, S.; Xue, Q.; Ma, X.; Wang, Y. *Arxiv:1011.1055*, 2010.

(13) Checkelsky, J. G.; Hor, Y.; Liu, M.; Qu, D.; Cava, R.; Ong, N. P. *Phys. Rev. Lett.* **2009**, *103* (24), 246601.

(14) Steinberg, H.; Gardner, D. R.; Lee, Y. S.; Jarillo-Herrero, P. *Nano Lett.* **2010**, *10*, 5032–5036.

(15) Lu, H.; Shan, W.; Yao, W.; Niu, Q.; Shen, S. *Phys. Rev. B* **2010**, *81*, 115407.

(16) Liu, C.; Zhang, H.; Yan, B.; Qi, X.; Frauenheim, T.; Dai, X.; Fang, Z.; Zhang, S. *Phys. Rev. B* **2010**, *81*, 041307.

(17) Linder, J.; Yokoyama, T.; Sudbø, A. *Phys. Rev. B* **2009**, *80*, 205401.

(18) Zhang, Y.; Chang, C.; Song, C.; Wang, L.; Chen, X.; Jia, J.; Fang, Z.; Dai, X.; Shan, W.; Shen, S.; Niu, Q.; Zhang, S.; Xue, Q. *Nat. Phys.* **2009**, *6*, 584–588.

(19) Murakami, S.; Nagaosa, N.; Zhang, S. *Phys. Rev. Lett.* **2004**, *93*, 156804.

(20) Kane, C. L.; Mele, E. J. *Phys. Rev. Lett.* **2005**, *95*, 226801.

(21) Bernevig, B. A.; Zhang, S. *Phys. Rev. Lett.* **2006**, *96*, 106802.

(22) Novoselov, K. S.; Jiang, D.; Schedin, F.; Booth, T. J.; Khotkevich, V. V.; Morozov, S. V.; Geim, A. K. *Proc. Natl. Acad. Sci. U.S.A.* **2005**, *104*, 10451–10453.

(23) Zhang, Y.; Tan, Y.; Stormer, H. L.; Kim, P. *Nature* **2005**, *438*, 201–204.

(24) Hirahara, T.; Sakamoto, Y.; Takeichi, Y.; Miyazaki, H.; Kimura, S.; Matsuda, I.; Kakizaki, A.; Hasegawa, S. *Phys. Rev. B* **2010**, *82*, 155309.

(25) Ayari, A.; Cobas, E.; Ogundadegbe, O.; Fuhrer, M. S. *J. Appl. Phys.* **2007**, *101*, 014507.